Sensors and Materials, Vol. 37, No. 8 (2025) 3577–3593
MYU Tokyo

S & M 4138

Adaptive Fuel Consumption Strategy Based on Operating Conditions of Plug-in Hybrid Electric Vehicles

Yan-Zuo Chang,[1] Tian-Syung Lan,[2] Zhi-Wei Zhang,[2] and Shi-Dong Li[1*]

[1]School of Energy and Power Engineering, Guangdong University of Petrochemical Technology, Maoming, Guangdong 525000, China
[2]College of Mechanical and Control Engineering, Guilin University of Technology, Gui Lin Shi, Guangxi 541004, China

(Received March 31, 2025; accepted June 24, 2025)

Keywords: ECMS, BP neural network, variable step length Firefly Algorithm, equivalence factor

For a hybrid vehicle, an appropriate energy management strategy is crucial to distribute the energy to satisfy the power performance of the vehicle. The plug-in hybrid electric vehicle (PHEV)'s driving conditions in Fuzhou, China were simulated in this study considering the power components, driver's habit, and dynamics module using Matrix Laboratory (MATLAB) and Simulink. In the simulation, the adaptive equivalent consumption minimization strategy (ECMS) simulation model was constructed. The equivalent factors for initial states of batteries, driving distances, and driving conditions were optimized using the variable-step Firefly Algorithm with an established library of optimal equivalent factors. A penalty function was introduced using the reference curve to dynamically adjust the equivalence factors in real time. The backpropagation neural network was used to build the Simulink model for driving condition determination, and its prediction accuracy reached 88.7%. Compared with the rule control strategy, adaptive ECMS improved the fuel economy by 7.77 and 4.48%. The results serve as a reference for developing an integration strategy for sensor data to enhance PHEV performance.

1. Introduction

For the energy management of hybrid vehicles, rule-based and optimization-based control strategies are used. Sensor technology is essential to develop an energy management strategy (EMS) for hybrid vehicles as collecting real-time data is crucial to optimize energy usage. Sensors are used to monitor the state of charge (*SOC*) and state of health (SOH) of the battery, engine speed, torque, and fuel consumption, and optimize torque distribution and energy efficiency.[1,2]

On the basis of sensor data, rule-based control strategies are established on deterministic and fuzzy rules while optimization-based control strategies are established on offline global optimization and online transient optimization. Peng *et al.* used a dynamic programming (DP) algorithm to optimize the range of engine operation using rule-based control strategies to reduce

*Corresponding author: e-mail: 1936532762@qq.com
https://doi.org/10.18494/SAM5663

ISSN 0914-4935

power and fuel consumption.[3] Ding *et al.* determined 12 different operating statuses in accordance with different power requirements in rule-based control strategies.[4] They used genetic algorithms (GAs) to optimize the parameters to reduce the emission of polluting gases.[4] Xu *et al.* used GA and DP algorithms to optimize the fuzzy control parameters to improve the fuel economy.[5] Bo *et al.* optimized the fuzzy rule parameters by using a quality-learning algorithm and a gradient descent method to shorten the computation time and enhance the fuel economy and vehicle dynamic performance.[6] Wang *et al.* applied the DP algorithm to a plug-in hybrid electric vehicle (PHEV) to calibrate fuel control strategies.[7] Zhang *et al.* adjusted the equivalence factor using a fuzzy proportional-integral controller and reduced the fuel consumption by 4.44%.[8] Wang *et al.* used a fuzzy logic controller to adjust the equivalence factor considering the deviation of the reference *SOC* from the measured *SOC* for fuel consumption saving.[7] However, with such control strategies, optimal values cannot be identified under different driving conditions, states, distances, and *SOC*s. In addition, identifying driving and engine conditions is important to enhance the effect of control strategies on the fuel economy.

Larsson *et al.* used the global positioning system (GPS) to determine the most economical driving routes using the reference *SOC* curve, and its fuel consumption was reduced by 1.9%.[9] Ye *et al.* predicted the vehicle speed in the next 10 s on the basis of vehicle network communication and adjusted the torque distribution on the basis of the prediction to effectively improve the vehicle fuel economy.[10] However, the recognition method is easily disturbed by the environment during vehicle driving, which makes it difficult to predict in a shorter time than using the conventional physics- or measurment-based method. Shen *et al.* proposed a new speed prediction algorithm using a Markov model and backpropagation neural network (BPNN) to compensate for the prediction errors. When applying the algorithm to a fuel consumption strategy and power maintenance strategy, fuel economy was improved by 3.11 and 7.93%, respectively.[11] Sun *et al.* proposed an improved control algorithm based on long and short-term memory (LSTM), and fuel was saved by 18.71%.[12] The previous algorithms required a huge amount of data for prediction, which caused biased model prediction in unexpected events.

Therefore, we identified driving conditions on the basis of previous vehicle movements and built a BPNN model. To overcome the disadvantage that the fixed equivalence factors do not apply to complex driving conditions, we used the Firefly Algorithm to construct the map of equivalence factors on the basis of initial states of batteries, driving distances, and driving conditions. An adaptive equivalent consumption minimization strategy (ECMS) was also formulated on the basis of the predicted driving conditions to obtain enhanced fuel economy compared with charge-depleting (CD) and ECMS strategies.

2. Model Design

In this study, a single-axle parallel PHEV of P2 type was used (Fig. 1). The universal characteristic curve of the PHEV was obtained by testing the engine at different speeds and torques, as shown in Fig. 2.

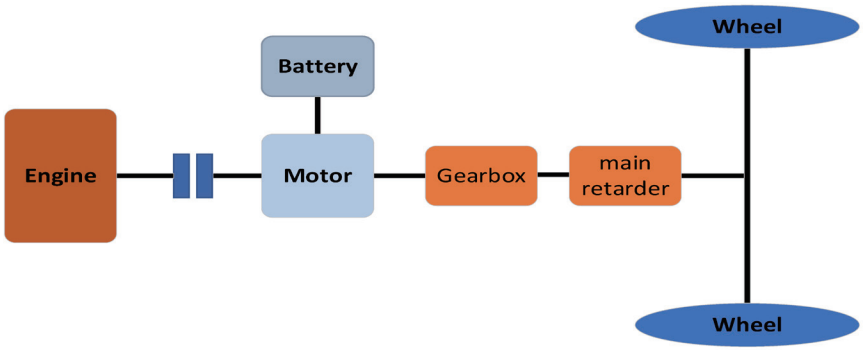

Fig. 1. (Color online) Structure of PHEV P2 type.

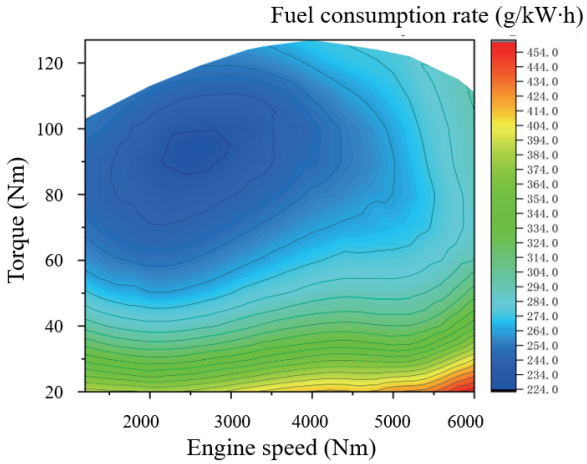

Fig. 2. (Color online) Universal characteristic curve of engine of PHEV P2 type.

The fuel consumption rates of the engine under the chosen speed and torque were calculated as

$$b_e = f_{e2}\left(n_e, T_e\right), \tag{1}$$

$$\dot{m}_f = \frac{P_e \cdot f_{e2}\left(n_e, T_e\right)}{\rho \cdot D \cdot 10}, \tag{2}$$

where b_e is the brake specific fuel consumption (BSFC), which is the rate of fuel consumption per unit of power output, f_{e2} is a function that relates the engine speed and torque to the BSFC, n_e is the engine speed (in RPM), T_e is the engine torque (in Nm), $\dot{m}_f$ is the mass flow rate of fuel consumption (in kg/s or g/s), P_e is the engine power (in W), ρ is the fuel density (in kg/m^3), D is the total distance driven, and 10 is a conversion factor. The efficiency curve of the PHEV was obtained by testing the motor at different speeds and torques, as shown in Fig. 3

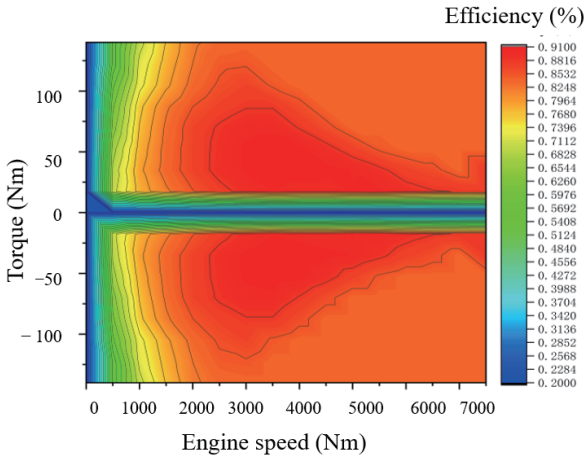

Fig. 3. (Color online) Motor efficiency curve.

The efficiency of the motor [Eq. (3)] and the charging and discharging power [Eq. (4)] under the chosen speed and torque were calculated.

$$\eta_m = f_{m2}\left(n_m, T_m\right) \tag{3}$$

$$P_{ele} = \frac{T_m \cdot n_m}{9550} \eta_m^{-sign(T_m)} \tag{4}$$

Here, η_m is the efficiency of the motor, f_{m2} is the function that describes the motor's efficiency based on its speed (n_m) and torque (T_m), P_{ele} represents the electrical power of the motor, and 9550 is a conversion constant.

We used the R_{int} model as an equivalent circuit model. The open circuit voltage and internal resistance and the *SOC* of the battery are used in the model (Figs. 4–6). Voltage and the charge states of batteries were estimated using Eqs. (5)–(8).

$$V_{bat} = V_{oc} - I_{bat} \cdot R_{int} \tag{5}$$

$$Voc = f\left(SOC\right) \tag{6}$$

$$R\begin{cases} R_{dis}\left(SOC\right), Discharge \\ R_{chg}\left(SOC\right), Charging \end{cases}_{int} \tag{7}$$

$$SOC = SOC_O - \frac{\int_0^t I_{bat} dt}{Q} \tag{8}$$

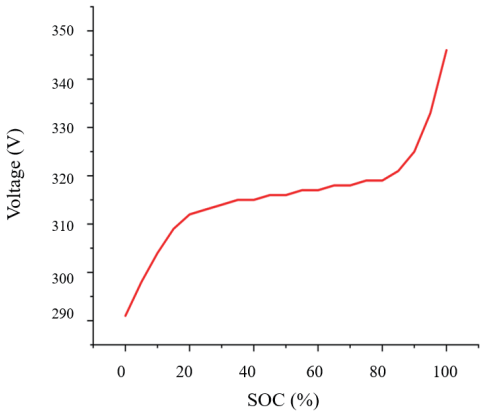

Fig. 4. (Color online) Open circuit voltage curve.

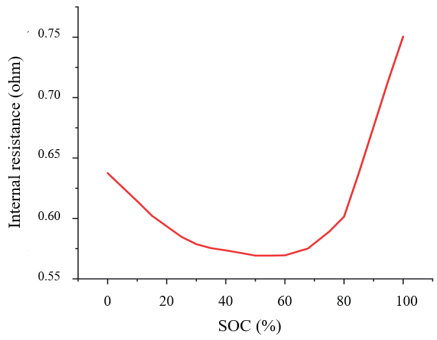

Fig. 5. (Color online) Charge internal resistance curve.

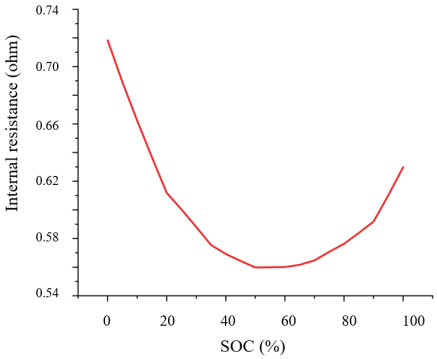

Fig. 6. (Color online) Discharge internal resistance change curve.

Here, V_{bat} is the battery terminal voltage, V_{oc} is the open circuit voltage, I_{bat} is the battery current (in A), R_{int} is the battery internal resistance (in Ω), R_{dis} is the internal resistance during discharge, and R_{chg} is the internal resistance during charging.

3. Adaptive ECMS

3.1 Control strategy

The principle of ECMS was proposed by Paganelli *et al.*[13] The objective function is transformed into an instantaneous optimization for each moment by using the objective function for real-time control. The equivalent fuel consumption is the sum of the engine fuel and motor power consumption.[14] In the PHEV, the battery is consumed in the CD and charging sustaining (CS) modes. In the CD mode, more power is consumed on the externally charged grid with a small equivalent factor. During driving, the vehicle tends to use the minimum power of the battery. The Pontryagin Minimum is used to minimize fuel consumption as long as the power demand is satisfied. In this study, engine torque was used as the control variable and electricity as the state variable in the state equations Eqs. (10) and (11).

$$\dot{m}_{equ} = \dot{m}_e + \dot{m}_m \tag{9}$$

Here, $\dot{m}_{equ}$ is the equivalent fuel consumption, $\dot{m}_e$ is the engine fuel consumption, and $\dot{m}_m$ is the motor equivalent fuel consumption.

$$\dot{SOC}(t) = f\left(SOC(t), T_e(t), t\right) = -\frac{I}{Q_{ess}} \tag{10}$$

$$I = \frac{U_{oc}\left(SOC(t)\right) - \sqrt{U_{oc}(SOC(t))^2 - 4R_b\left(SOC(t)\right)\cdot P_{bat}(t)}}{2R_b\left(SOC(t)\right)} \tag{11}$$

I is the battery current, Q_{ess} is the battery capacity, U_{oc} is the open-circuit voltage, R_b represents the internal resistance, and $P_{bat}(t)$ is the battery power.

The constraint conditions are defined as

$$\begin{cases} SOC_{min} \le SOC(t) \le SOC_{max} \\ n_{m\_min} \le n_m(t) \le n_{m\_max} \\ n_{e\_min} \le n_e(t) \le n_{e\_max} \\ T_{m\_min}(t) \le T_m(t) \le T_{m\_max}(t) \\ T_{e\_min}(t) \le T_e(t) \le T_{e\_max}(t) \end{cases}, \tag{12}$$

where SOC_{min} and SOC_{max} are the upper and lower limits of battery power, n_{m_min} and n_{m_max} are the minimum and maximum speeds of the motor, n_{e_min} and n_{e_max} are the minimum and maximum speeds of the engine, $T_{m\_min}(t)$ and $T_{m\_max}(t)$ are the minimum and maximum torques

of the motor at a given moment, and $T_{e\_min}(t)$ and $T_{e\_max}(t)$ are the minimum and maximum torques of the engine at a given moment, respectively.

The target performance equation is

$$\min J = \int_{t_0}^{t_f} \dot{m}_e\left(SOC(t), T_e(t)\right) dt\,. \tag{13}$$

The Hamiltonian function equation (14) is used by multiplying the objective function with the derivatives of the state variables by the Lagrange multipliers.

$$H\left(SOC(t), T_e(t), t\right) = \dot{m}_e\left(T_e(t)\right) + \lambda(t) \cdot \dot{SOC}(t) \tag{14}$$

Here, $\dot{m}_e$ represents the instantaneous fuel consumption rate of the engine and $\lambda(t)$ is the Lagrange multiplier.

From the optimal solution at each moment, the global optimal solution is obtained, and in the Pontryagin minimum, the system satisfies the canonical equation:

$$\dot{\lambda}(t) = -\frac{\partial H}{\partial x} = \lambda(t) \frac{\partial}{\partial SOC}\left[\frac{U_{oc}\left(SOC(t)\right) - \sqrt{U_{oc}(SOC(t))^2 - 4R_b\left(SOC(t)\right) \cdot P_{bat}(t)}}{2R_b\left(SOC(t)\right) Q_{ess}}\right], \tag{15}$$

where Q_{ess} is the battery capacity.

During driving, the battery is charged and discharged, and its power P_{bat} has positive and negative values alternately. The Hamiltonian functions Eqs. (16) and (17) are used to describe the states of charging and discharging.

$$H\left(SOC(t), T_e(t), t\right) = \dot{m}_e\left(T_e(t)\right) + S(t) \cdot \frac{P_{bat}}{Q_{lhv} \cdot \eta_{bat}} \quad P_{bat} \geq 0 \quad P_{bat} \geq 0 \tag{16}$$

$$H\left(SOC(t), T_e(t), t\right) = \dot{m}_e\left(T_e(t)\right) + S(t) \cdot \frac{P_{bat} \cdot \eta_{bat}}{Q_{lhv}} \quad P_{bat} < 0 \quad P_{bat} < 0 \tag{17}$$

Here, η_{bat} is the instantaneous charging and discharging efficiency of the battery power and Q_{lhv} is the low heating value of fuel.

3.2 Firefly Algorithm

The standard Firefly Algorithm has a search process to find local optimal solutions and minimize the discovery steps of global optimal solutions. The numbers of steps in the Firefly Algorithm are adjusted for optimization. At the beginning of the iteration of the algorithm, more steps are used to search for the global optimal point. As the algorithm iterates, the number of

necessary steps decreases to quickly converge to the global optimum and improve the accuracy of the algorithm. The algorithm flow is as follows.

(1) Initialize the basic parameters. Set the number of firefly individuals N, the step factor α, the absorption coefficient of the medium to light γ, the maximum attraction β_O, the maximum number of iterations T_{max}, and the randomly generated firefly positions.

(2) Calculate the adaptation value of each firefly as its respective brightness in accordance with the firefly location [Eq. (18)].

$$f(x) = \int_0^t m_e dt \tag{18}$$

(3) Calculate the attraction between fireflies using

$$R_{ij} = \sqrt{(x_j - x_i)^2}\ , \tag{19}$$

$$\beta_R = \beta_O e^{\left(-\gamma \cdot R_{ij}^{\ 2}\right)}, \tag{20}$$

where R_{ij} is the distance between two fireflies i and j, and β is the attractiveness of a firefly at a certain distance R_{ij}, e is Euler's number, and γ is the light absorption coefficient.

(4) Update its position using Eq. (21). The low luminance is affected by the high-luminance firefly.

$$x_i^{'} = x_i + \beta_R\left(x_j - x_i\right) + \alpha\varepsilon \tag{21}$$

x_i is the position of firefly i in space, ε is the random perturbation whose value is between −0.5 and 0.5, α is a randomization parameter or step size factor, and ε is a random number (or vector of random numbers) drawn from a Gaussian (normal) distribution.

(5) Reduce the step size factor to improve the merit-seeking ability using

$$\alpha = k \cdot \alpha\ , \tag{22}$$

where k is the variable step coefficient.

(6) Record the population fitness value, i.e., the optimal objective function value, and the optimal individual position as numerical parameters.

(7) Determine whether the iteration reaches the maximum number of iterations. If not, procedures (2)–(6) are repeated; otherwise, (8) is executed.

(8) Output the optimal value of each parameter.

Using the typical driving conditions in Fuzhou City, the optimal equivalent factor library of initial power and driving distance was established for three driving conditions. In the conditions,

the initial power levels were configured to range from 30 to 80%, increasing incrementally by 10%, and the driving distances were 90, 70, 50, and 30 km. The optimal factors were found to be integrated into the library, as shown in Figs. 7–9.

3.3 *SOC* penalty function

For the battery power to approach its lower limit toward the end of driving, a penalty function and reference *SOC* curves were developed to optimize performance. The reference *SOC* curve shows a straight line. *SOC*s in predriving (SOC_0), in the lower battery limit (SOC_f), and the total driving distance h are presented in Fig. 10.

When the vehicle is driven, *SOC* does not decrease below the reference curve with the *SOC* penalty function P_{SOC} [Eq. (22)].

$$\Delta SOC = \frac{1}{5 \times \left(1 + e^{2 \times P_{SOC}}\right)} - 0.1 \tag{22}$$

Here, ΔSOC is the difference between the reference *SOC* and the actual *SOC* of the car at a certain moment.

The penalty function with the equivalence factor forms the new equivalent fuel consumption expression:

$$\dot{m}_{equ} = \dot{m}_e + (S + P_{SOC}) \cdot \dot{m}_m \,. \tag{23}$$

The penalty factor P_{SOC} changes depending on the battery discharge capacity and the difference between the reference and actual *SOC*s for the maximized utilization of battery power and the optimized fuel consumption.

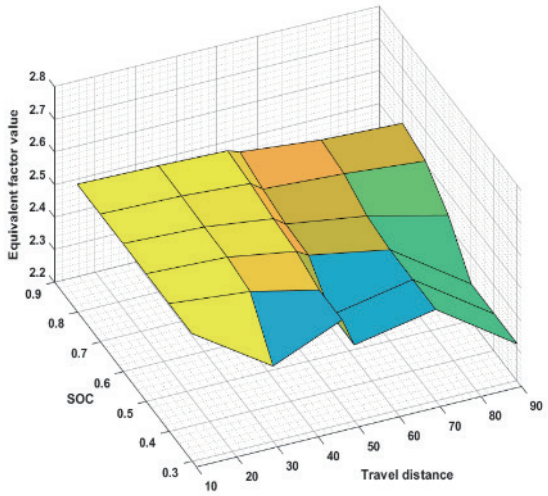

Fig. 7. (Color online) Optimal equivalent factor library for low-speed driving.

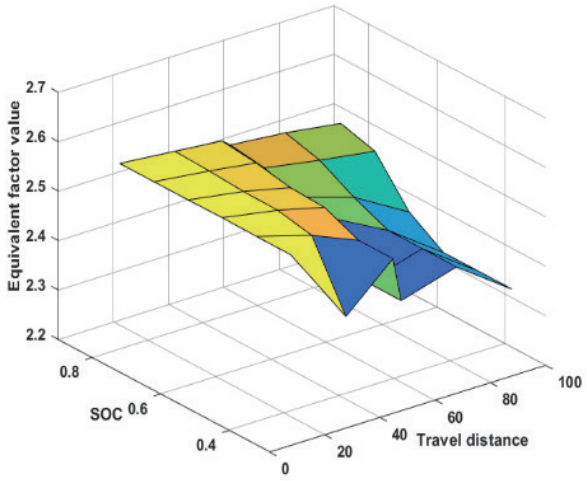

Fig. 8. (Color online) Optimal equivalent factor library for intermediate-speed driving.

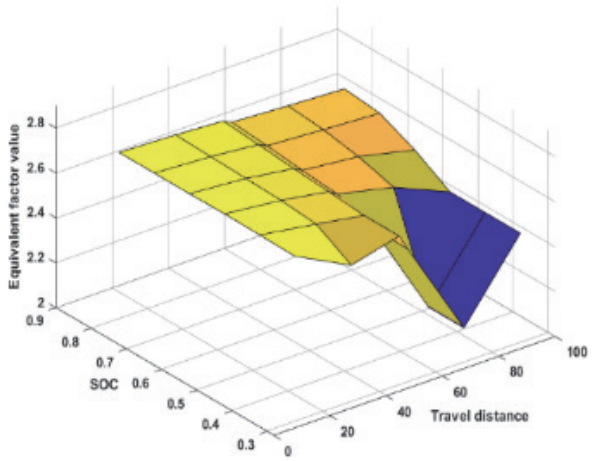

Fig. 9. (Color online) Optimal equivalent factor library for high-speed driving.

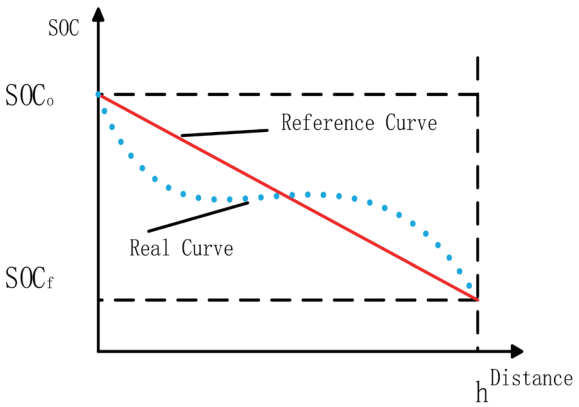

Fig. 10. (Color online) Reference *SOC* curve.

3.4 BPNN

Three hundred data values were randomly selected for the speed ranges to extract features from the training samples for BPNN (Table 1). The receiver operating characteristic (ROC) curve, confusion matrix, and the best performance are shown in Figs. 11–13, respectively. The classification result from the ROC curve is presented in Fig. 11. The confusion matrix presents the prediction accuracies of 88.8, 95.2, and 90.5% for three driving conditions, and the overall accuracy of 89.3%, which meets the requirements. In the best performance, the cross-entropy is 0.07196. The measured output is close to the predicted output, indicating the excellent performance of BPNN.

4. Simulation Results

To verify the effectiveness, adaptive ECMS was simulated, and the result was compared with those of the fixed equivalent fuel consumption strategy and the rule control strategy. The urban driving conditions in Fuzhou were combined in a driving time of 12000 s. Figure 14 shows the results of the driving conditions. The simulation results of adaptive ECMS at different speeds are presented in Fig. 15. The error range was 1.5, which meets the requirement for optimal driving.

Figures 16 and 17 show the *SOC* and engine torque in the CD and CS modes in the rule control strategy. In the CD mode, the motor provides additional power to the engine, which consumes too much battery power. In the CS mode, the engine provides power for the whole vehicle and consumes power to charge the battery. In the CS mode, a longer driving time and better fuel consumption than in the CD model were observed. The adaptive ECMS does not

Table 1
Training samples.

Serial number	Type of driving condition	Maximum speed (km/h)	Average speed (km/h)	Average acceleration speed of acceleration section (m/s^2)	Average deceleration speed of deceleration section (m/s^2)	Driving condition category
1	Low speed	12.3	5.305	0.370	−0.418	001
2	Low speed	34.6	15.381	0.372	−0.478	001
			:			
100	Low speed	7.433	1.864	0.314	−0.346	001
101	Mid-speed	64.733	32.062	0.546	−1.045	010
102	Mid-speed	47.433	24.876	0.383	−0.511	010
			:			
200	Mid-speed	53.767	30.123	0.581	−0.583	010
201	High speed	93.067	45.704	0.516	−0.613	100
			:			
300	High speed	50.767	32.053	0.291	−0.463	100

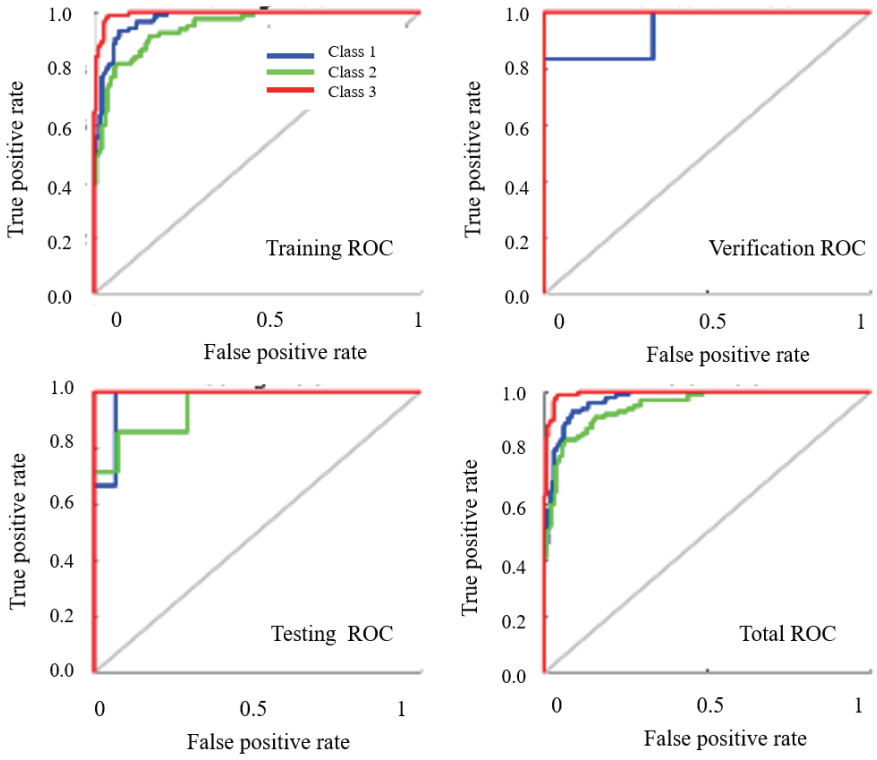

Fig. 11. (Color online) ROC curves.

Target class	Output class 1	Output class 2	Output class 3	Row total
1	77 (28.8%)	10 (3.8%)	0 (0.0%)	88 (11.5%)
2	11 (4.1%)	87 (26.0%)	9 (3.3%)	107 (17.3%)
3	0 (0.0%)	5 (1.9%)	85 (31.8%)	94 (8.4%)
Column total	87 (32.5%)	102 (38.2%)	94 (35.1%)	283 (100.0%)

Training confusion matrix

Target class	Output class 1	Output class 2	Output class 3	Row total
1	6 (2.3%)	0 (0.0%)	0 (0.0%)	6 (100.0%)
2	0 (0.0%)	11 (5.2%)	0 (0.0%)	11 (100.0%)
3	1 (4.8%)	0 (0.0%)	4 (19.0%)	5 (20.0%)
Column total	7 (33.3%)	11 (10.5%)	4 (19.0%)	22 (95.2%)

Verification confusion matrix

Target class	Output class 1	Output class 2	Output class 3	Row totals
1	6 (28.6%)	2 (9.5%)	0 (0.0%)	8 (75.0%)
2	0 (0.0%)	5 (23.8%)	0 (0.0%)	5 (100.0%)
3	0 (0.0%)	0 (0.0%)	6 (21.1%)	6 (100.0%)
Column total	6 (100.0%)	7 (28.6%)	6 (21.1%)	19 (90.5%)

Test confusion matrix

Target class	Output class 1	Output class 2	Output class 3	Row total
1	6 (2.3%)	0 (0.0%)	0 (0.0%)	6 (100.0%)
2	0 (0.0%)	11 (5.2%)	0 (0.0%)	11 (100.0%)
3	1 (4.8%)	0 (0.0%)	4 (19.0%)	5 (20.0%)
Column total	7 (33.3%)	11 (10.5%)	4 (19.0%)	22 (95.2%)

Total confusion matrix

Fig. 12. Confusion matrices.

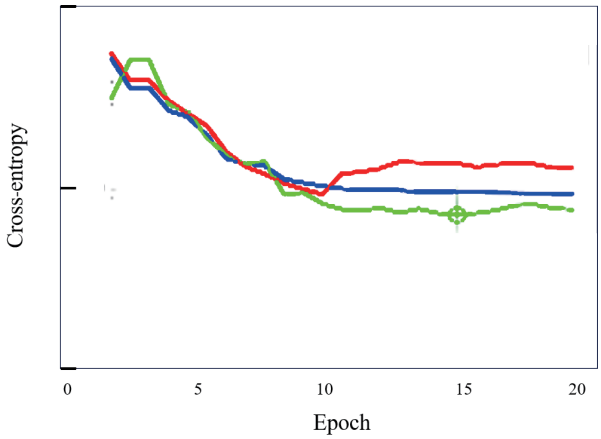

Fig. 13. (Color online) Best validation performance (0.07198) in epoch 18 (red line: training, blue line: verification, green line: testing result).

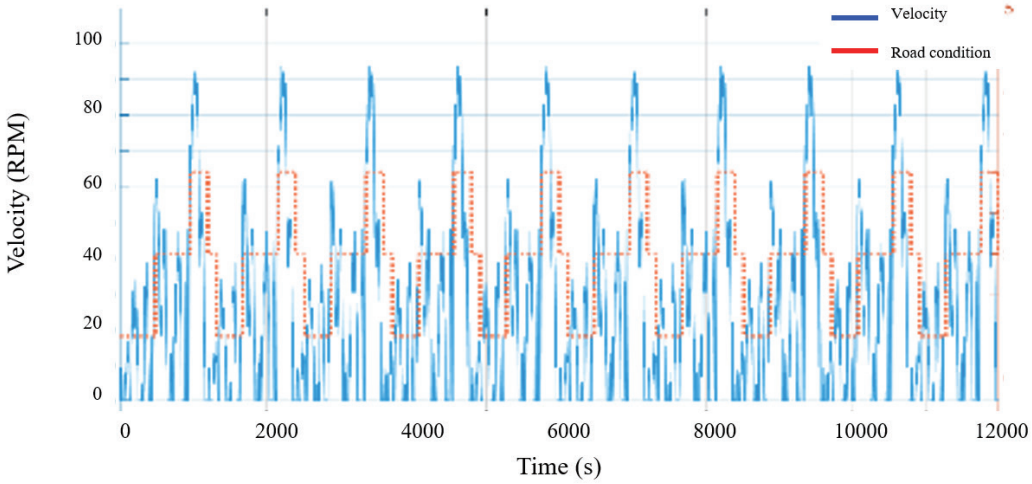

Fig. 14. (Color online) Combined driving conditions in simulation.

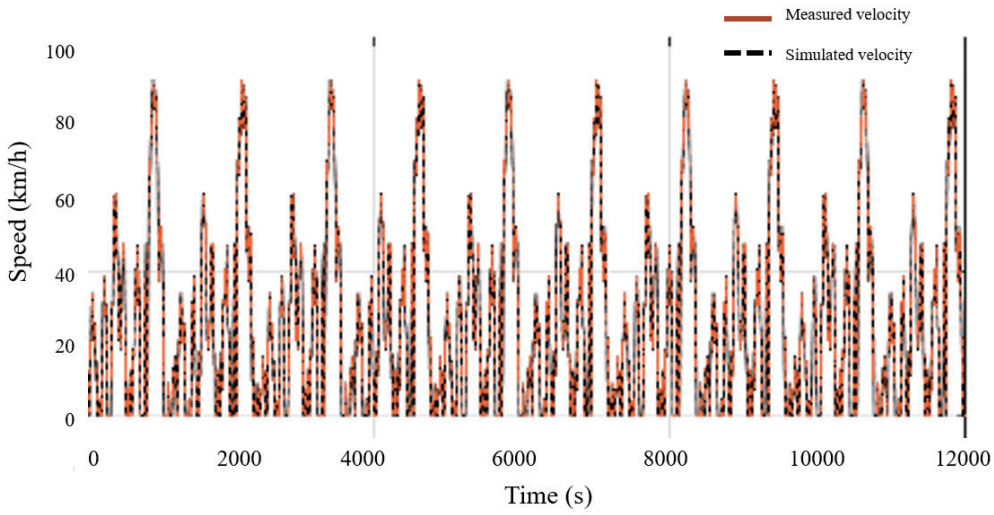

Fig. 15. (Color online) Simulation results of adaptive ECMS.

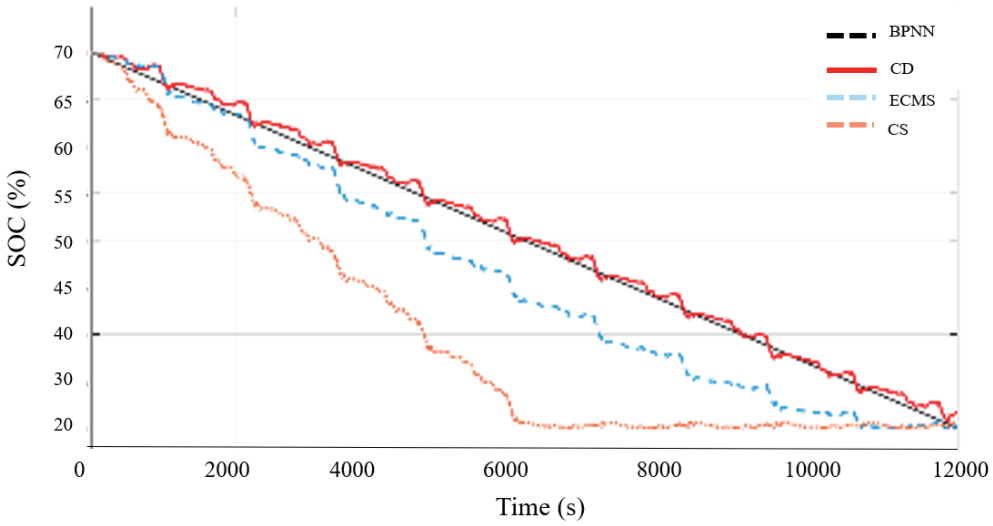

Fig. 16. (Color online) SOC in CD and CS modes.

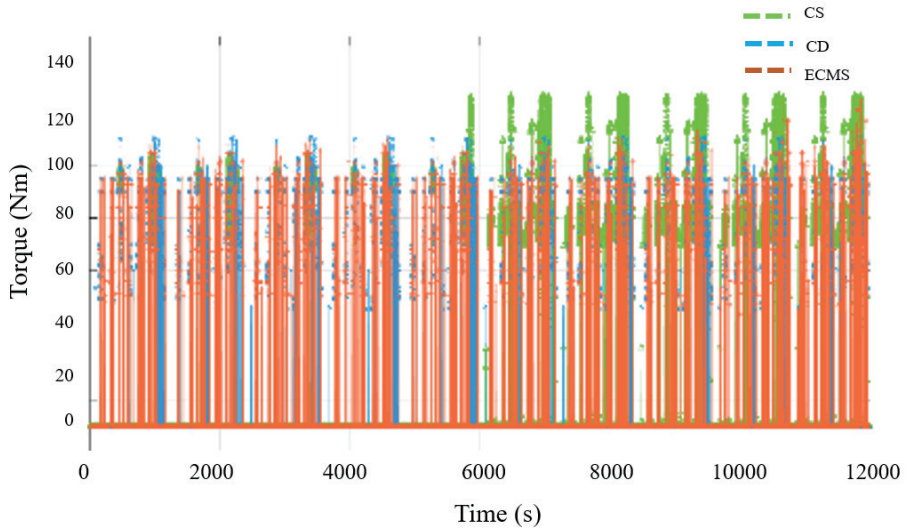

Fig. 17. (Color online) Engine torque in CD and CS modes.

dynamically select the equivalent factor to the changing conditions and initiates the CS mode. In adaptive ECMS, the changing conditions during driving are identified to dynamically select the equivalent factor. At the same time, the penalty function is used with a new equivalent factor. In the CD mode, the power of the engine and the motor is fully utilized to avoid the execution of the CS mode by distributing the engine and motor torque efficiently.

Figure 18 shows the fuel consumption of the three energy control strategies throughout the whole driving process. In ECMS, after the CS mode is initiated, the engine increases its fuel consumption rapidly. In adaptive ECMS, the power is evenly used throughout the driving

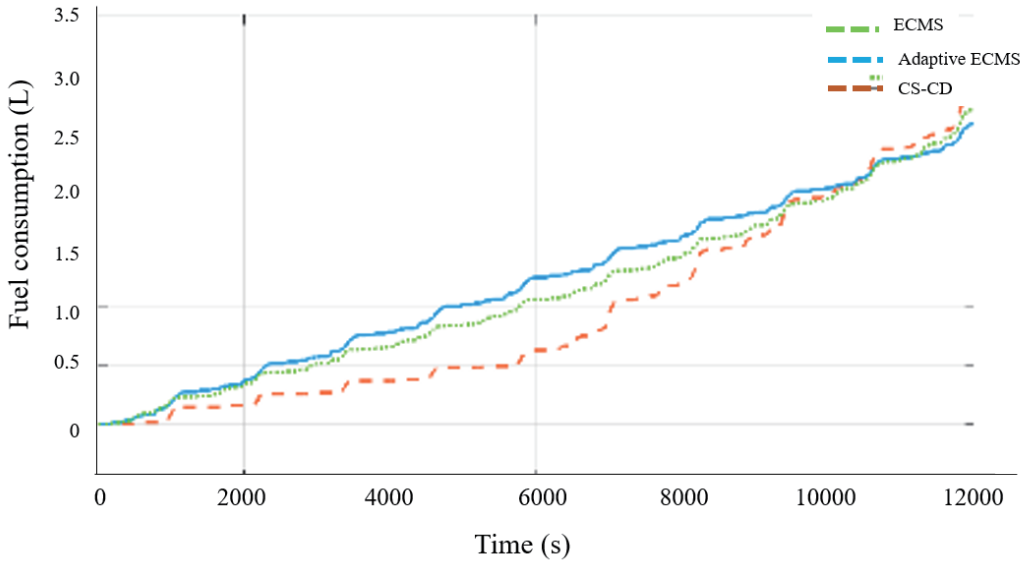

Fig. 18. (Color online) Cumulative fuel consumption curve.

process, and the engine torque is reasonably distributed to achieve efficient driving and reduce fuel consumption.

The fuel economy with ECMS was improved by 3.44% in 100 km driving while adaptive ECMS improved the fuel economy by 7.77% (Table 2). Adaptive ECMS reduced fuel consumption most effectively under the driving conditions of Fuzhou.

5. Sensor Technology for Adaptive Fuel Consumption Strategy

Sensor technology plays a pivotal role in enhancing the fuel economy of ECMS in PHEVs by providing real-time, accurate data, which is essential for optimal energy management. As highlighted in the results of this study, sensors must be used to monitor the battery's *SOC* and SOH, engine speed, torque, and fuel consumption for optimizing torque distribution and energy efficiency. To refine the adaptive ECMS by providing richer contextual data, more precise and dynamic adjustments of the equivalence factor are required.

In this study, while BPNN achieves a commendable prediction accuracy of 88.7% for driving conditions, incorporating a wider array of sensor data significantly improves the accuracy and robustness of such predictions, leading to even greater fuel economy. To advance the model of this study, which was developed on the basis of past vehicle movements to identify driving conditions, Lidar and radar sensors must be used to collect precise data about traffic density, road curvature, and upcoming obstacles.[15,16] This data can be fed into BPNN to accurately estimate future power demands, allowing ECMS to pre-emptively adjust the engine and motor operation. GPS data integrated with live traffic information through connected vehicle systems or external data feeds enables ECMS to predict stop-and-go conditions or periods of high-speed driving with greater certainty.[10] Such accurate prediction allows for intelligent battery management and engine operation.

Table 2
Fuel consumption economy.

Control strategy	Cumulative fuel consumption (L)	Fuel consumption per 100 km (L/km)	Economic improvement (%)
Rule control	2.785	3.282	–
ECMS	2.69	3.169	3.44
Condition recognition adaptive ECMS	2.57	3.027	7.77

Other than Lidar, radar, and GPS data, data on road surface conditions (e.g., wet, icy, or rough) needs to be used to enable the powertrain to save power.[17] By inputting the data into ECMS, power delivery can be adjusted to reduce traction and optimize efficiency. Exhaust gas composition data (e.g., NOx, CO_2, and particulate matter) and optimal battery temperature are important information on engine combustion efficiency and emissions[18] and the efficiency and longevity of the battery.

These data must be used to sustain appropriate fuel economy over the vehicle's lifespan and to select the most efficient combination of engine and motor power delivery in ECMS. For ECMS improvements, effective data fusion from multiple sensors is mandatory. For instance, real-time vehicle speed, acceleration, and GPS data with traffic predictions and road conditions need to be combined and processed by sophisticated machine learning algorithms, to achieve precise and adaptive equivalence factor adjustments. The robust adaptive ECMS of this study can be advanced with the integration of sensor data, coupled with sophisticated data fusion and predictive analytics to further improve the fuel economy of PHEVs.

6. Conclusions

Using MATLAB/Simulink, we built a simulation model of PHEV driving. On the basis of the principle of Pontryagin's minima, adaptive ECMS was built in MATLAB with the engine torque as the control variable, the power as the dependent variable, and the size of the equivalent factor *S*. Fuel consumption depends on the initial battery state, driving distance, and driving conditions. The optimal equivalence factors were obtained by using variable steps at different speeds. To fully utilize the battery power and adjust the equivalence factor in real time, a penalty function was created. Three hundred data values under various driving conditions were randomly selected to train BPNN, and the prediction accuracy reached 89.3% with a cross-entropy of 0.07196, indicating satisfactory performance. Three different control strategies in CD and CS modes showed the fuel consumptions of 3.0271/100 (adaptive ECMS), 3.282/100 (rule control strategy), and 3.169/100 (ECMS) (L/km). The fuel economy of ECMS and adaptive ECMS was improved by 4.48 and 7.77%, respectively, compared with that of the rule control strategy. The results of this study provide a reference to formulate an integration strategy of sensor data for the improvement of PHEV performance.

References

1 V. Mitta and R. Shah: World Electr. Veh. J. **15** (2024) 424. https://doi.org/10.3390/wevj15090424
2 N. Xu, Y. Kong, L. Chu, H. Ju, Z. Yang, Z. Xu, and Z. Xu: Appl. Sci. **9** (2019) 2026. https://doi.org/10.3390/app9102026
3 J. K. Peng, H. W He, and R. Xiong: Appl. Energy **185** (2017) 1633. https://doi.org/10.1016/j.apenergy.2015.12.031
4 N. Ding, K. Prasad, and T. T. Lie: Int. J. Energy Res. **45** (2021) 1627. https://doi.org/10.1002/er.5808
5 Q. W. Xu, X. X. Luo, X. B. Jiang, and M. Zhao: Iet Electr. Syst. Tran. **8** (2018) 144. https://doi.org/10.1049/iet-est.2017.0067
6 L. Bo, L. J. Han, C. L. Xiang, H. Liu, and T. Ma: Energy **252** (2022) 123976. https://doi.org/10.1016/j.energy.2022.123976
7 X. M. Wang, H. W. He, F. C. Sun, and J. L. Zhang: Energies **8** (2015) 3225. https://doi.org/10.3390/en8043225
8 F. Q. Zhang, H. O. Liu, Y. H. Hu, and J. Q. Xi: Energies **9** (2016) 919. https://doi.org/10.3390/en9110919
9 V. Larsson, L. Johannesson, B. Egardt, and A. Lassson: Proc. American Control Conf. (ACC, 2012). https://doi.org/10.1109/ACC.2012.6314910
10 M. Ye, J. Chen, X. Li, K. Ma, and Y. G. Liu: Sensors **21** (2021) 5370. https://doi.org/10.3390/s21165370
11 P. H. Shen, Z. G. Zhao, X. W. Zhan, J. W. Li, and Q. Y. Guo: Energy **155** (2018) 838. https://doi.org/10.1016/j.energy.2018.05.064
12 X. L. Sun, J. Q. Fu, H. Y. Yang, M. K. Xie, and J. P. Liu: Energy **269** (2023) 126772. https://doi.org/10.1016/j.energy.2023.126772
13 G. Paganelli, S. Delprat, T. M. Guerra, J. Rimaux, and J. J. Santin: IEEE 55th Vehicular Technol. Conf. (2002) 2076–2081. https://doi.org/10.1109/VTC.2002.1002989
14 S. H. Wang, X. S. Huang, J. M. Lopez, X. Y. Xu, and P. Dong: IEEE Access **7** (2019) 133290. https://doi.org/10.1109/ACCESS.2019.2941399
15 S. Gupta, A. K. S. Tripathi, and S. Tripathi: IEEE Trans. Intell. Transp. Syst. (2024) 1. https://doi.org/10.1109/TITS.2024.3476132
16 E. D. Saldivar-Carranza, J. Desai, A. Thompson, M. Taylor, J. Sturdevant, and D. M. J. Bullock: Sensors **24** (2024) 6410. https://doi.org/10.3390/s24196410
17 N. Rosenberger and M. Lienkamp: IJEETC **13** (2024) 494. https://www.ijeetc.com/vol13/IJEETC-V13N6-494.pdf
18 T. J. Wallington, J. E. Anderson, R. H. Dolan, and S. L. Winkler: Atmosphere **13** (2022) 650. https://doi.org/10.3390/atmos13050650